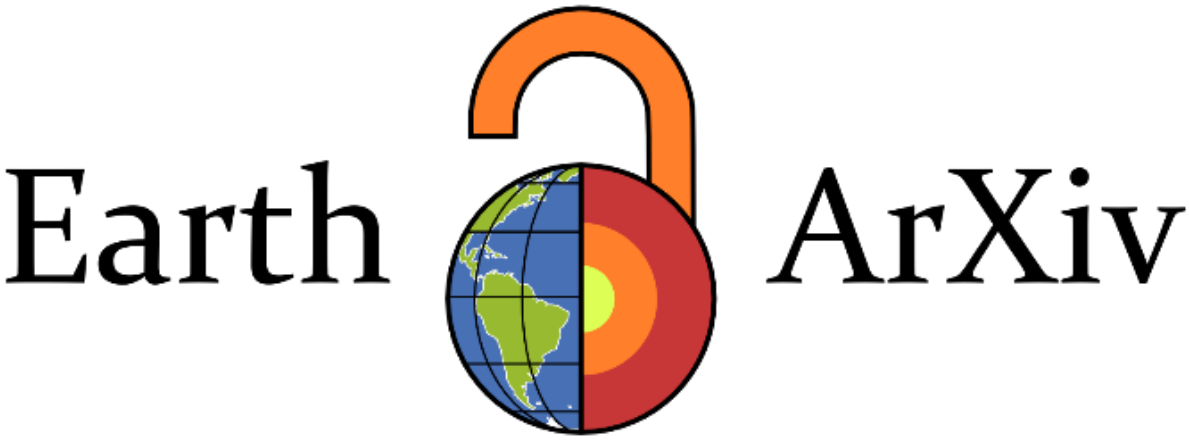

Detection, Classification, and Characterization of Compound Coastal Flooding along the Gulf and Southeastern U.S. Coasts

Samrin S. Sauda [1], Manzhu Yu [1, 2]*

[1] Department of Geography, College of Earth and Mineral Sciences, The Pennsylvania State University; [2] Institute of Energy and the Environment, The Pennsylvania State University

* Corresponding author: mqy5198@psu.edu

Highlights

- First observation-based compound flood typology for the Gulf-Southeast US coast
- Five-type compound coastal floods including synchronous, lagged, antecedent are identified on the basis of surge-discharge interactions.
- Compound coastal flood fraction varies four-fold across sub-regions; peaks align with active hurricane seasons
- Lagged compound events show 2-day routing lag, basis for 48-hour compound flood advisory
- Joint intensity hotspots uncorrelated with event frequency

Abstract

Compound coastal flooding, driven by the concurrent or sequential exceedance of storm surge and river discharge thresholds, poses disproportionate risk to Gulf and Southeast US coastal communities, yet systematic observation-based characterization of its spatial distribution, typological structure, and joint intensity remains limited. This study investigates compound coastal flooding using a nonstationary threshold-based detection framework applied to 72 paired USGS-NOAA gauge stations over 2010-2024. Station-level flood events were identified and classified into five mutually exclusive types based on driver exceedance and surge-discharge timing lag: surge-only, riverine-only, compound-synchronous, compound-lagged, and compound-antecedent events. Results show that surge-only events dominate the regional flood record, accounting for 58.7% of events, followed by riverine-only events at 31.4%, while compound events represent 9.9%. Compound flood occurrence varies strongly across sub-regions, with the highest compound fraction observed in the Pascagoula-Mobile-Tombigbee region and distinct lagged and antecedent behavior in the Florida Panhandle and Southeast Atlantic Coast, respectively. Annual compound fractions show pronounced interannual variability, with elevated values during active or impactful hurricane seasons. Compound events also persist substantially longer than surge-only events, indicating greater cumulative exposure. Overall, this study provides an observation-based physically interpretable framework for identifying compound coastal flood typologies and demonstrates the

importance of incorporating event timing, joint intensity, and regional hydrologic controls into coastal flood risk assessment, early warning, infrastructure design, and adaptation planning.

Keywords: compound flood; coastal flood; storm surge; river discharge; Southeast Atlantic Coast; Gulf Coast.

1 Introduction

Anthropogenic warming, accelerating sea level rise, and expanding coastal urbanization have driven a marked increase in compound flooding over the past century, particularly in major coastal cities (Ezer & Atkinson, 2014; Little et al., 2015; Moftakhari et al., 2017). Compound flooding occurs when multiple flood drivers such as elevated coastal water levels, heavy precipitation, and increased river discharge, coincide or closely follow one another. This generates inundation magnitudes and extents that routinely exceed what any individual driver would produce in isolation, and imposing socioeconomic impacts that overwhelm infrastructure designed for single-driver events (Zscheischler et al., 2018; Visser-Quinn et al., 2019). Seneviratne et al. (2021) concludes with medium to high confidence that compound flood probability has already increased at many locations and will continue to intensify as sea levels rise and precipitation extremes deepen, particularly in association with tropical cyclone precipitation. Bevacqua et al. (2020) further projected that under high-emissions scenarios, the co-occurrence probability of surge and rainfall extremes could increase globally by more than 25% by 2100, with compound flooding becoming more than 2.5 times as frequent at latitudes above 40°N, underscoring the urgency of improved characterization and prediction for vulnerable coastal populations.

This study focuses on compound coastal flooding, typically arising from three primary drivers: river discharge (fluvial), precipitation-induced surface runoff (pluvial), and coastal processes including storm surge, astronomical tides, wave action, and relative sea-level rise. The physical mechanisms underlying these interactions are well established but operate nonlinearly, with distinct driver configurations carrying fundamentally different implications for early warning and flood modelling. In estuarine environments, elevated coastal water levels and high river discharge combine to raise water surfaces beyond inundation thresholds that neither driver could reach independently. Even moderate surge events that would not independently cause coastal flooding can obstruct gravity-driven stormwater drainage, exacerbating concurrent precipitation-driven inundation (Ward et al., 2018; Yangchen et al., 2021; Xu et al., 2023). Under tropical cyclone conditions, surge and discharge often peak near-simultaneously as a single storm generates extremes across the entire coastal-riverine system (Couasnon et al., 2020; Ghanbari et al., 2021; Gori & Lin, 2022). Because these mechanisms interact nonlinearly, compound flood risk is systematically underestimated when drivers are modelled in isolation (Wahl et al., 2015; Bevacqua et al., 2017).

Two interrelated gaps constrain the scientific foundation for compound flood risk assessment. First, the field has historically lacked a coherent typological framework - a gap Zscheischler et al. (2020) explicitly identified as the motivation for the first comprehensive compound event classification, organizing events into four categories: preconditioned, multivariate, temporally compounding, and spatially compounding. The absence of such a framework limits the capacity to design suitable modelling approaches and develop

effective adaptation strategies, given that a large and growing proportion of climate-related impacts arise from compounding rather than single drivers (Zscheischler et al., 2018; Raymond et al., 2020). Additionally, most studies reduce this complexity to a binary compound/non-compound classification based on joint exceedance probability, underestimating the temporal structure of driver interactions and the distinct risk implications of different compound subtypes. Second, observational constraints severely limit what is known about historical compound flood occurrence. Studies built on directly observed data remain scarce, with most compound flood research dominated by numerical simulation, statistical modelling, and reanalysis-based approaches (Couasnon et al., 2020; Juárez et al., 2022; Sohrabi et al., 2025). Simultaneous observations of multiple flood drivers are sparse in both space and time (Green et al., 2025) and as a result, the frequency, typology, and spatial distribution of historically observed compound flood events at the gauge-network scale remain poorly characterized. Ali et al. (2025) explicitly note that it remains unknown how many historically recorded flood events were compound rather than single driver in nature.

These gaps are especially acute along the Gulf and Southeastern U.S. coasts, a region that concentrates compound flood risk more acutely than almost any other under both current and projected climate conditions (Ghanbari et al., 2021; Wahl et al., 2015). Compound flood research in this region has grown substantially since the pioneering work of Wahl et al. (2015), with notable contributions from (Moftakhari et al., 2017, 2019), (Muñoz et al., 2020, 2021), Ghanbari et al. (2021), Nasr et al. (2021), Gori & Lin, (2022), and Ali et al. (2025). The region's elevated exposure reflects the occurrence of frequent Gulf-landfalling tropical cyclones, large drainage basins producing substantial riverine responses, and rising sea levels that progressively lower the threshold for coastal inundation. Gori & Lin (2022) demonstrated through numerical modelling that by 2100, the frequency of joint extreme surge and rainfall events could increase 7- to 36-fold in the southern United States, driven by decreasing tropical cyclone translation speed and increasing storm intensity. Ali et al. (2025) found that across 168 of 203 coastal counties examined along the Gulf and Atlantic coasts, over 70% of all recorded flood events were compound in nature, with compound occurrence rates reaching 90-100% in counties spanning Louisiana to Florida's Panhandle and along the Southeast Atlantic seaboard. Despite this elevated exposure and documented compound flood frequency, systematic observation-based spatiotemporal characterization of compound flood across this remains poorly studied.

This study addresses both gaps through a comprehensive observation-based compound flood characterization framework applied to the Gulf Coast and Southeast United States over the period 2010-2024. There are two primary objectives associated with this study. First, to detect and classify compound coastal flood events across paired USGS-NOAA gauging stations on the basis of resolving surge-discharge interactions. Second, to systematically characterize the spatiotemporal distribution, interannual variability, and joint flood intensity of compound coastal flood events, producing a network-scale flood catalogue for this region grounded in directly observed gauge records. Together, these objectives advance the understanding of compound coastal flood dynamics along the Gulf and Southeastern U.S. coasts using directly observed gauge records. This complements existing model-based assessments by providing station-level empirical evidence for the spatiotemporal heterogeneity, and typological diversity of compound coastal flooding, and offering a physically grounded foundation for more targeted early warning systems, improved infrastructure design standards, and better-informed adaptation decisions in one of the most compound-flood-prone coastal regions in the United States.

2 Data Source and Methodology

2.1 Study Area and Data Sources

The study domain encompasses the Gulf and Southeast Atlantic region of the United States, extending from the Louisiana Delta to the Georgia-South Carolina coast (approximately 79°W-94°W, 24°N-35.5°N; Figure 1; Table 1). The domain was subdivided into four sub-regions based on station clusters and at HUC4 scales: (1) Pascagoula-Mobile-Tombigbee, (2) Florida Panhandle, (3) Peace-Tampa Bay, and (4) SE Atlantic Coast, reflecting distinct combinations of coastal morphology, catchment characteristics, and storm exposure.

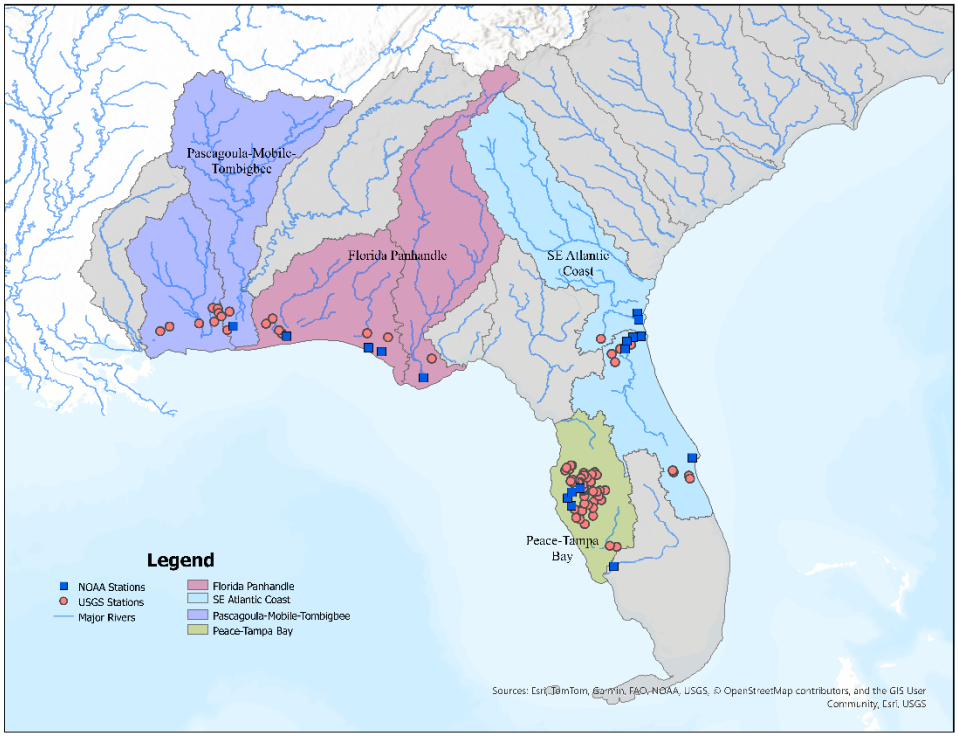

Figure 1. Study area showing 72 USGS gauging stations, paired with 17 NOAA tide gauges. and four geographic sub-regions.

Table 1: List of sub-regions across Southeast Atlantic and Gulf coasts

Sub-region	**HUC 4 Region**	**State**	**Area (km^2)**	**No of Stations**
SE Atlantic Coast	St. Johns + Altamaha-St. Marys	FL	85223	9
Peace-Tampa Bay	Peace-Tampa Bay	FL	27515	46
Florida Panhandle	Choctawhatchee-Escambia+ Apalachicola	FL	93849	7

Pascagoula-Mobile-Tombigbee	Pascagoula + Mobile-Tombigbee	AL,LA, MS	88562	10

Because this study focuses on compound coastal flooding, we examine the interaction between two primary coastal flood drivers: coastal storm surge and river discharge. Past studies have shown a strong and increasing statistical dependence between storm surge and heavy precipitation/river discharge along the United States coasts (Wahl et al., 2015; Moftakhari et al., 2017; Ward et al., 2018; Couasnon et al., 2020; Nasr et al., 2021). For e.g. Wahl et al. (2015) found significant dependency between surge and precipitation in the Gulf and Southeast coasts.

Hourly river discharge data were obtained from U.S. Geological Survey (USGS) gauging stations, while hourly storm surge observations were derived from National Oceanic and Atmospheric Administration (NOAA) coastal tide gauges between 2010-2024. Each USGS station was paired with its nearest NOAA station within 50 km, yielding 283 unique USGS-NOAA pairs. This distance threshold was chosen to ensure that both the riverine and coastal observations represent the same coastal drainage environment or estuarine influence zone. Previous compound flood studies have used comparable proximity criteria for tide gauge-river station pairing. Li et al. (2026) selected USGS river discharge stations using a maximum distance of 55 km (0.5°) between the river outlet and tidal gauge, while Ghanbari et al. (2021) selected paired NOAA-USGS stations when eligible USGS stations were located within 100 km of NOAA tidal stations. Thus, the 50 km threshold used here provides a conservative pairing criterion that is consistent with existing compound coastal flood literature while ensuring that paired stations represent nearby coastal-watershed interactions

The discharge records were obtained from 72 USGS stations, selected based on record completeness (≥ 90%), low fraction of negative discharge, and in proximity to NOAA tide gauges. Hourly tidal heights were obtained from 17 NOAA coastal stations; storm surge was estimated as the meteorological residual after removal of predicted astronomical tide using NOAA's tidal prediction model, yielding daily maximum surge residuals for compatibility with streamflow records (Moftakhari et al., 2017; Sweet et al., 2022)

$$Surge\ (S) = Tidal\ Height_{Observed} - Tidal\ Height_{Predicted}$$

2.2 Threshold Definition and Event Classification

Flood thresholds were defined independently for discharge (τ_Q) and storm surge (τ_S) at each station. Daily maximum discharge from USGS gauges and daily maximum surge from NOAA tide gauges were extracted for each station pair over the 2010-2024 study period. A day was flagged as a threshold exceedance when either or both drivers exceeded their respective station-specific thresholds - days on which both drivers simultaneously exceeded their thresholds were designated as compound coastal flood days (Figure 2). Thresholds were defined as the 97th percentile of a rolling 365-day window, consistent with compound flood studies applying 95th-99th percentile criteria for co-occurring extremes (Bevacqua et al., 2019; Couasnon et al., 2020; Ghanbari et al., 2021). The 365-day rolling window provides a locally adaptive baseline that captures seasonal flood cycles and reduces sensitivity to nonstationary changes in the distribution of extremes (Vogel et al., 2011; (Salas & Obeysekera, 2014).This a nonstationary formulation that accommodates secular trends in sea-level rise and precipitation regimes rather than

imposing a fixed historical percentile (Bevacqua et al., 2019; Couasnon et al., 2020; Vogel et al., 2011; Zscheischler et al., 2018). A fixed threshold is inappropriate here because both discharge and surge distributions are demonstrably nonstationary over the study period, and applying a static percentile would confound shifts in the threshold itself with changes in flood events frequency. Flood events are separated by fewer than three days below threshold and were merged into a single event window following Ghanbari et al. (2021). A three-day merging window was applied because compound flood impacts often persist across successive days, and short gaps below this duration are more likely to represent one extended hydrometeorological episode than independent events.

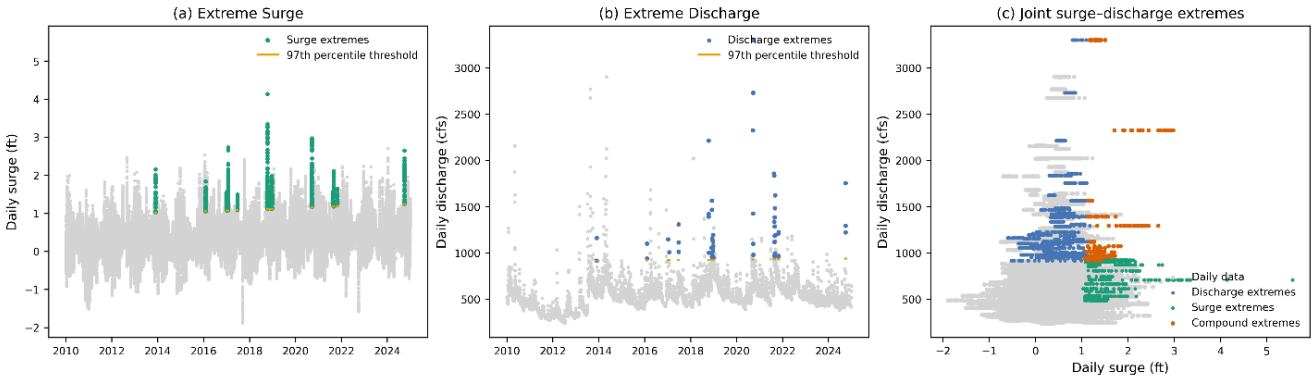

Figure 2. Detection of extreme and compound surge-discharge events for a USGS-NOAA station pair (a) Daily surge values with a dynamically varying 97th-percentile threshold used to identify surge extremes. (b) Daily streamflow with its corresponding 97th-percentile threshold used to detect discharge extremes

Compound coastal flood events were classified into five mutually exclusive event types (Figure 3) based on two criteria: whether the flood drivers exceeded their thresholds, and the timing lag δt between their peak occurrences.

$$Timing\ Lag\ (\delta t) = t(Q_{peak}) - t(S_{peak}) \quad (1)$$

where $t(Q_{peak})$ is the time of the daily maximum discharge peak, and $t(S_{peak})$ is the time of the daily maximum surge peak. A positive δt indicates that discharge peaks after surge (river-first), a negative δt indicates that discharge peaks before surge (surge-first), and $\delta t \approx 0$ indicates near-simultaneous peaking of both drivers.

While many compound flood studies implicitly assume that peak drivers occur simultaneously or synchronously, several studies have demonstrated that the relative timing of these drivers can substantially influence the magnitude of extreme water levels and resulting flood impacts (e.g., Gori et al., 2020; Juárez et al., 2022). For example, an event in which surge and discharge peak within the same 24-hour window under tropical cyclone forcing is mechanistically distinct from one where discharge arrives two days after surge has already receded, reflecting catchment routing delay. Therefore, incorporating timing structure as a classification dimension rather than simply identifying all co-exceedances as compound events, reflects a central argument of this study: that the temporal relationship between surge and discharge peaks is not merely a statistical artefact, but a physically meaningful characteristic that governs the flood-generation mechanism, event duration, and risk implications of a compound flood event.

This motivated the development of a five-type taxonomy that resolves the temporal structure of surge-discharge interaction into operationally and physically meaningful categories: surge-only, riverine-only, compound-synchronous, compound-lagged, and compound-antecedent (Figure 3; Table 2). Surge-dominant events ($S > \tau_S$, $Q \leq \tau_Q$) occur when surge exceeds the threshold (τ_S) due to wind and pressure forcing alone, while river discharge remains below its threshold (τ_Q). In contrast, river-dominant events ($Q > \tau_Q$, $S \leq \tau_S$) are characterized by discharge exceeding τ_Q due to rainfall or snowmelt without coastal forcing, with surge remaining below τ_S. Compound events involve both variables exceeding their thresholds and can be further categorized based on timing: compound-synchronous events (both exceed, $|\delta t| \leq 1$ day) occur when surge and discharge peaks are nearly simultaneous, often associated with tropical cyclone forcing (Wahl et al., 2015); compound-lagged events (both exceed, $\delta t > +1$ day) arise when surge precedes discharge, reflecting catchment travel-time delays as rainfall takes time to route through the river network; and compound-antecedent events (both exceed, $\delta t < -1$ day) occur when discharge precedes surge, representing pre-conditioning scenarios in which prior riverine flooding or soil saturation amplifies the impact of subsequent coastal surge (Leonard et al., 2014; Bevacqua et al., 2019).

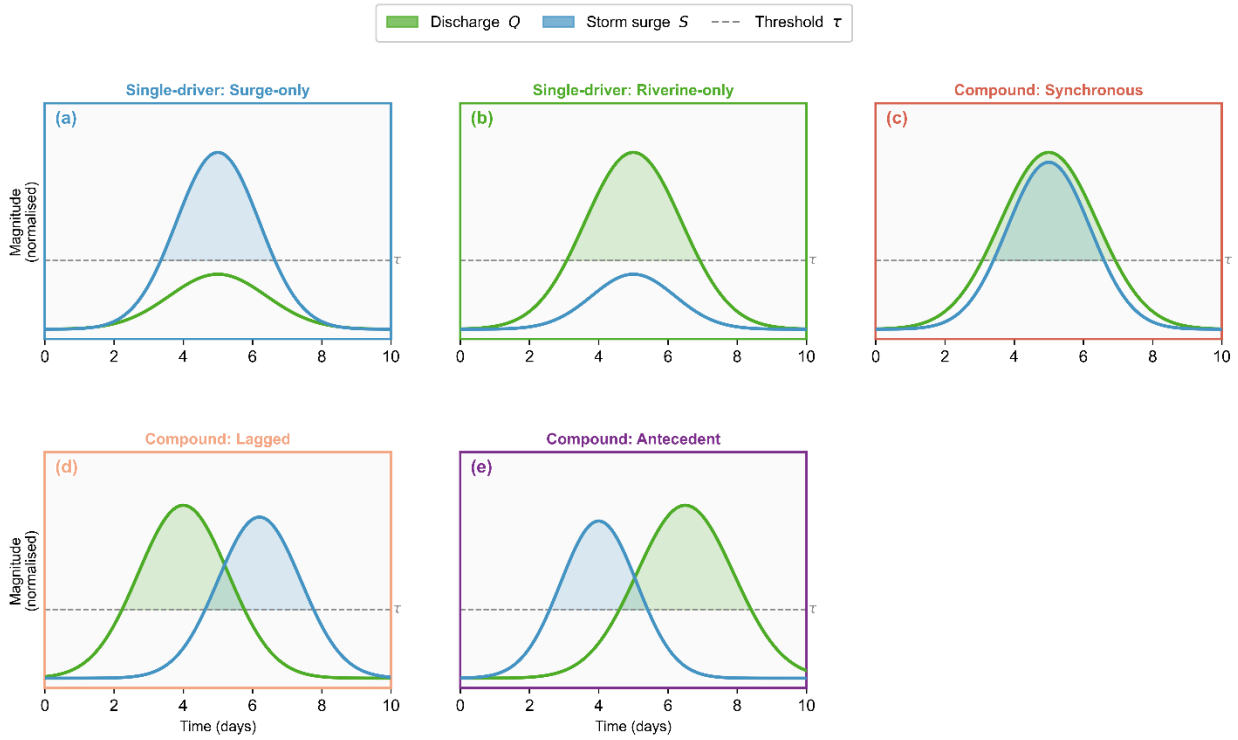

Figure 3. Classification of compound coastal flood events based on threshold exceedance and timing lag between peak surge and discharge

Table 2: List of compound coastal flood typology. N/A indicates that δt is not applicable for single-driver events where only one threshold is exceeded.

Event Type	$> \tau_S$	$> \tau_Q$	**δt**
Surge-dominant	Yes	No	N/A
River-dominant	No	Yes	N/A

Compound-synchronous (Co-occurring)	Yes	Yes	≤ 1 day
Compound-lagged (Discharge follows surge)	Yes	Yes	> +1 day
Compound-antecedent (Surge follows discharge)	Yes	Yes	< -1 day

2.3 Flood Intensity Metric

Joint flood intensity I_{joint} was computed as the normalized sum of exceedance magnitudes above station-specific thresholds, with the non-exceeding driver term set to zero for single-driver events:

$$I_{joint} = (Q_{peak} - \tau_Q)/\tau_Q + (S_{peak} - \tau_S)/\tau_S \quad (2)$$

where Q_{peak} is the daily maximum river discharge, S_{peak} is the daily maximum water level, and τ_Q and τ_S are the corresponding nonstationary 97th percentile thresholds for discharge and surge respectively.

Each term represents the fractional exceedance of a driver above its local threshold, a value of zero when the threshold is not exceeded, and a positive value proportional to how far above the threshold the driver peaked. The two terms are summed up to produce a single dimensionless intensity metric (I_{joint}) that captures both the magnitude and the multi-driver character of each flood event. For a purely surge-driven event, the discharge term is zero and I_{joint} reduces to the surge exceedance fraction alone; for a compound event, both terms contribute, producing a higher I_{joint} than either driver would generate independently.

This formulation follows the exceedance-based normalization approach established for joint flood driver quantification at regional and global scales (Couasnon et al., 2020; Sadegh et al., 2018; Wahl et al., 2015; Ward et al., 2018). The dimensionless, station-normalized metric enables cross-site comparison across gauges with substantially different absolute discharge and surge magnitudes, consistent with composite index approaches applied along the US Gulf and East coasts (Ali et al., 2025) and in global delta systems (Eilander et al., 2020).

3 Results

3.1 Spatial Distribution of Compound Coastal Flood Typology

A total of 37,847 station-level flood episodes were detected across the 72-station network over 2010-2024, corresponding to approximately 767 unique domain-level storm events (1-day temporal grouping window) along the Gulf and Southeastern U.S. coasts. The results reveal that the domain is dominated by single-driver events (Figure 4). Across all sub-regions, a consistent pattern emerged, with surge-dominated events most frequently, followed by riverine and then compound flood events. Surge-only events accounted for the largest share (n = 22,230; 58.7%), consistent with the predominantly coastal and estuarine character of the gauge network. Riverine-only events represented 31.4% of the total (n = 11,887), reflecting discharge threshold exceedances driven by precipitation without concurrent surge influence. Compound flood events accounted for 9.9% of all events (n = 3,730) and occurred across all four sub-regions. Within the compound category, synchronous events overwhelmingly dominated (n =

3,189; 85.5%), with lagged (n = 436; 11.7%) and antecedent (n = 105; 2.8%) subtypes comprising the remainder.

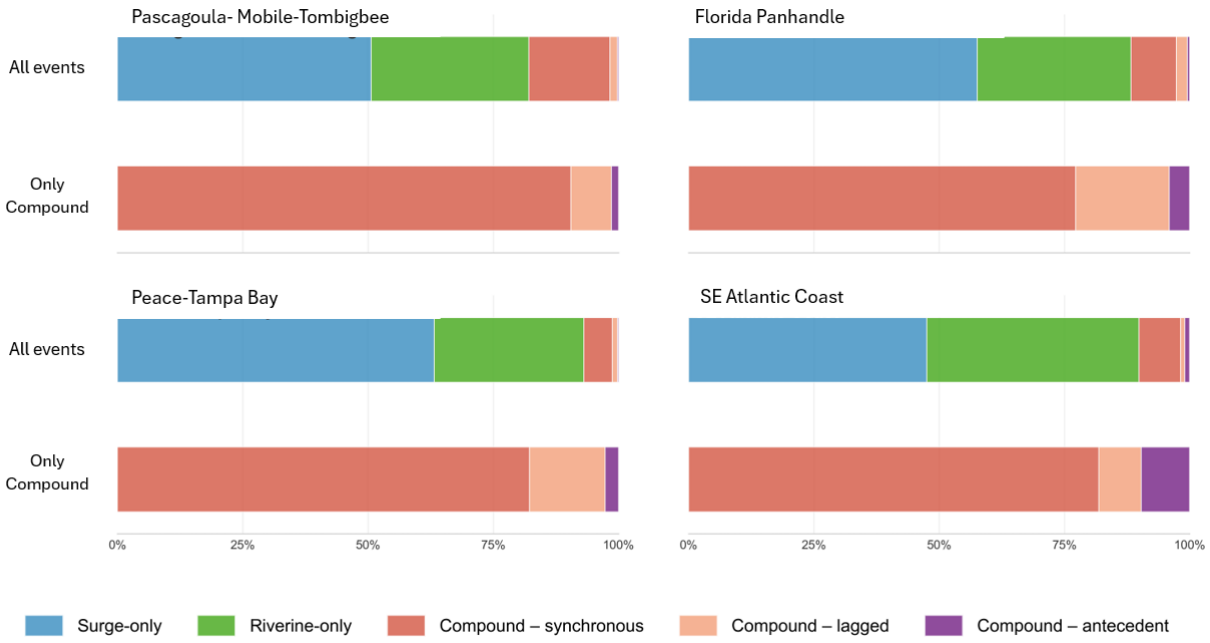

Figure 4. Proportional composition of compound coastal flood types across the sub-regions. Upper bar: all flood events; lower bar: compound events only.

Compound flood fraction exhibited pronounced spatial heterogeneity across the four sub-regions, ranging from 7% in the Peace-Tampa Bay watershed to 18% in the Pascagoula/Mobile-Tombigbee watershed (Fig. 4). This is a nearly threefold range demonstrating the inadequacy of domain-aggregated statistics for characterizing compound flood risk. The Pascagoula/Mobile-Tombigbee sub-region recorded the highest compound fraction (n = 1,566; 18%) and was overwhelmingly synchronous in its compound character (90%) followed by lagged events (8%). This sub-region was with surge-only events accounting for only 51% of total events, the second lowest surge dominance of any sub-region and the highest riverine contribution (31%), reflecting the hydrological importance of large inland drainage basins in this watershed. The Florida Panhandle sub-region exhibited an intermediate compound fraction (11%), with a notably elevated lagged fraction (19% of compound events). The Peace-Tampa Bay sub-region, while containing 46 of 72 stations and accounting for 65.2% of all events (n = 24,664), exhibited the lowest compound fraction (7%), and highest surge-only events (63%). Finally, the SE Atlantic Coast sub-region exhibited the most balanced surge-riverine distribution of any sub-region (48% surge-only, 42.3% riverine-only), and a 10 % compound fraction. This region also has the highest antecedent subtype fraction (1.0% of all events, equivalent to approximately 10% of regional compound events).

3.2 Interannual Variability in Compound Coastal Flood Frequency

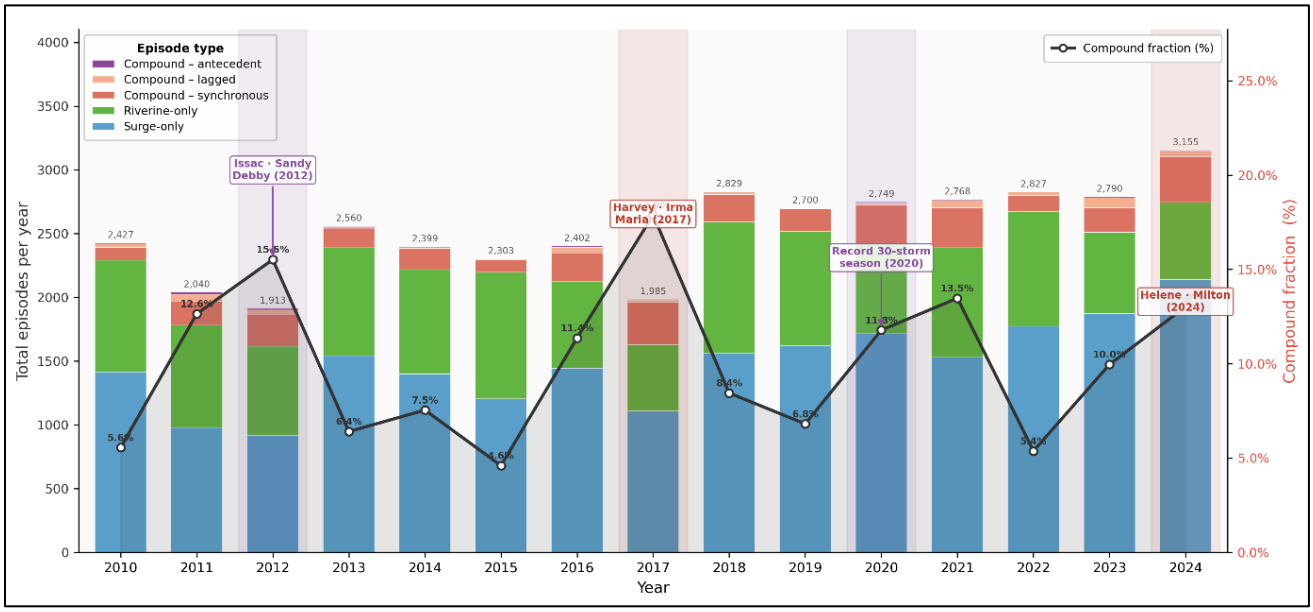

Figure 5. Annual compound fraction time series (2010-2024), and hurricane season annotations. Major hurricane years were annotated manually based on NOAA storm records to aid interpretation of interannual variability.

Total annual compound coastal flood events across the 72-station network ranged from 1,913 in 2012 to 3,155 in 2024 over the 2010-2024 study period (Fig. 5). The stacked bar composition reveals a consistently surge-dominated record in every year, with surge-only and riverine-only events collectively accounting for most annual totals across all years. The absolute event count shows a modest increasing tendency in the latter half of the record - total events in 2021-2024 averaged 2,885 per year compared to 2,265 per year in 2010-2014. Annual compound fractions ranged from 4.6% (2015) to 17.9% (2017) - a nearly four-fold range reflecting dominant tropical cyclone influence.

The temporal pattern indicates that compound flooding is not proportional to total flood frequency. For example, 2015 and 2022 exhibit moderate-to-high total flood counts (>2,300 events) but low compound fractions (<6%), whereas 2017 shows the highest compound fraction despite having one of the lowest total events (1,985 events). Five distinct peak years are identifiable: 2012 (15.5%), 2017 (17.9%), and a sustained elevated period from 2020-2021 (11.8% and 13.5% respectively), followed by recovery to 13.0% in 2024. Three trough years: 2015 (4.6%), 2019 (6.8%), and 2022 (5.4%) represent periods of substantially reduced compound co-occurrence despite comparable or higher total event counts.

3.3 Compound Event Timing Structure and Duration

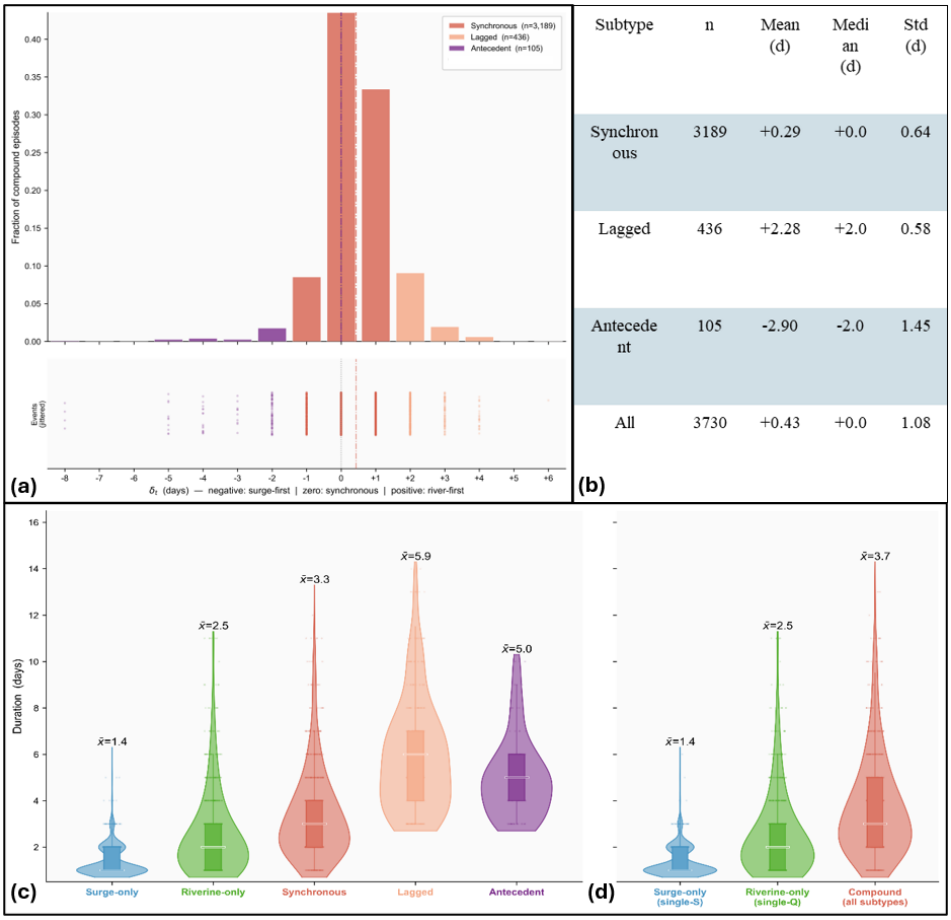

Subtype	n	Mean (d)	Median (d)	Std (d)
Synchronous	3189	+0.29	+0.0	0.64
Lagged	436	+2.28	+2.0	0.58
Antecedent	105	-2.90	-2.0	1.45
All	3730	+0.43	+0.0	1.08

Figure 6. (a) & (b) δt distribution by compound subtype with summary statistics table (c) Violin plots of flood duration for all five event types. (d) Grouped violin plots comparing flood duration between single-driver and compound events.

The distribution of timing lag (δt) across all compound flood events is displayed over the range -5 to +5 days (Fig. 6a). The distribution is strongly right-skewed and multimodal, with a domain-wide mean of +0.43 days and median of 0.00 days, confirming that synchronous and lagged (surge-first) timing are the dominant modes across the station network. The histogram reveals three visually distinct components: a dominant spike centered at δt = 0 and δt = +1 representing synchronous events, a secondary cluster at δt = +2 to +4 days representing lagged events, and a lower-magnitude negative grouping at δt = -1 to -5 days representing antecedent events. The rug plot in the lower panel (Fig. 6b) corroborates this structure - a dense near-continuous band at δt = 0, a compact scatter cluster near -2 days, and dispersed individual points between +2 and +4 days. Lagged events with a narrow-spread produce secondary modes and antecedent events produce small but identifiable bars with the widest spread of any subtype as revealed by the rug plot below.

Flood duration increases systematically across all five event types, following a statistically consistent hierarchy (Fig. 6c&d). Surge-only events exhibit the shortest duration (median = 1 day, mean = 1.4 days, max = 6 days), concentrated almost entirely below 3 days with a compact bottom-heavy violin and minimal upper tail. Riverine-only events are approximately twice as long (median = 2 days, mean = 2.5 days, max = 11 days), with a wider violin extending to 11 days. Among compound subtypes, all three categories substantially exceed single-driver durations. Synchronous events (median = 3 days, mean = 3.3

days, max = 13 days) produce a broad violin spanning 2-8 days with an upper tail reaching 13 days. Antecedent events (median = 5 days, mean = 5.00 days, max = 10 days) form a compact but elevated distribution concentrated between 4 and 7 days. Lagged events exhibit the longest duration of any subtype (median = 6 days, mean = 5.91 days, max = 14 days) with the widest IQR of all types (approximately 4-7 days), and the only subtype reaching 14 days in the record. At the aggregate level, the grouped compound distribution (mean = 3.7 days) has a mean duration 2.6 times that of surge-only events and 1.5 times that of riverine-only events, with the compound violin substantially wider throughout the 3-8-day range, confirming that compound events occupy a qualitatively distinct duration regime.

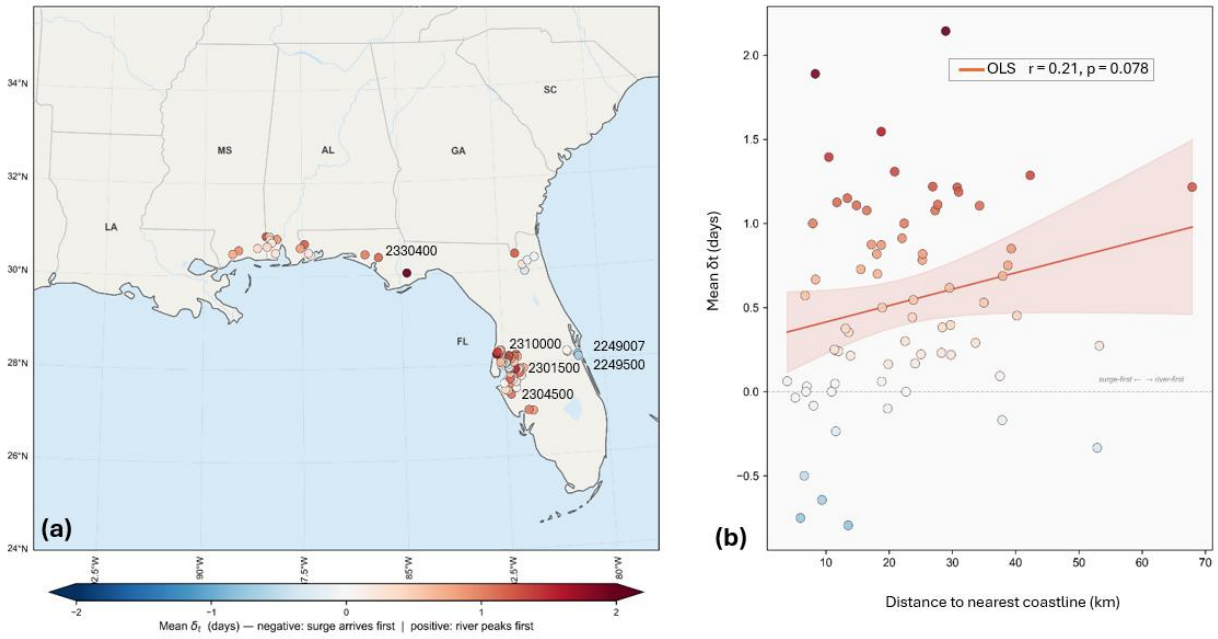

Figure 7. (a) Spatial distribution of mean compound event timing lag (δt) and top-3 and bottom-3 stations (δt). (b) δt vs Distance to Coast (km).

The spatial distribution of mean δt reveals a predominantly river-first signal across the domain, with warm-toned stations covering the Pascagoula-Mobile-Tombigbee, Florida Panhandle, and Peace-Tampa Bay (station mean = +0.53 ± 0.59 days, median = 0.00 days; Fig. 7a). The observed range spans -0.79 to +2.14 days across the 72-station network and the highest positive δt values are concentrated along the Florida Panhandle, with station 2330400 exhibiting the maximum recorded lag (+2.14 days), followed by stations 2310000 (+1.89 days) and 2301500 (+1.55 days) within the Peace-Tampa Bay vicinity. In contrast, the only surge-first stations (negative δt) in the network cluster within the SE Atlantic: stations 2304500 (-0.79 days), 2249007 (-0.75 days), and 2249500 (-0.64 days) - all located within approximately 10 km of the coastline.

Panel (b) shows a positive but marginally non-significant relationship between mean δt and distance to the nearest coastline (OLS r = +0.21, p = 0.078), with the wide 95% confidence interval and substantial residual scatter at all distance bands confirming that coastal distance is a weak and insufficient predictor of compound event timing on its own. The most anomalous station 2330400 (δt = +2.14 days) at only ~20 km from the coast, sits substantially above the regression line, indicating catchment-specific hydrological controls that coastal proximity alone cannot capture, while several stations at intermediate distances (30-

50 km) show near-zero or negative δt, further illustrating that gauge positioning within the tidal-fluvial transition zone governs timing at the individual station level more than absolute coastal distance.

3.4 Joint Flood Intensity and Spatial Hotspots

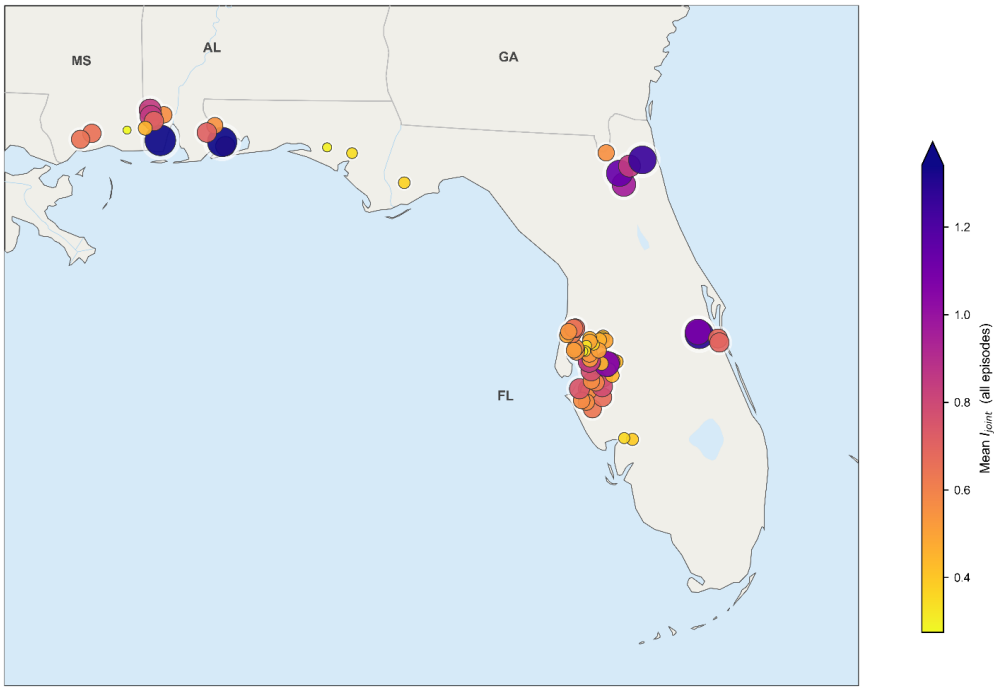

Figure 8. Mean I_{joint} map with station dots and top-5 intensity labels.

The mean I_{joint} map reveals pronounced spatial heterogeneity across the study domain, with high-intensity stations standing out clearly against a background of moderate-to-low values (Fig. 8). The Pascagoula/Mobile-Tombigbee sub-region records the highest I_{joint} values in the network**,** visible as large, dark purple circles along the MS/AL Coast**,** with peak station values of 1.49 and 1.38, forming the primary intensity hotspot of the domain. A secondary hotspot emerges along the SE Atlantic Coast, represented by two large purple circles on the northern Florida Atlantic seaboard (station values of 1.25 and 1.14) and a notably large purple circle near 28.5°N (I_{joint} = 1.29), confirming the SE Atlantic Coast as a distinct high-intensity zone despite its lower compound fraction. In contrast, the Peace-Tampa Bay sub-region**,** which contains the densest station cluster in the network**,** exhibits predominantly small, yellow-to-orange circles consistent with low mean I_{joint} values (approximately 0.4-0.7). The Florida Panhandle sub-region shows sparse small-to-medium circles in the yellow-orange range, reflecting intermediate I_{joint} values in the inter-station zone between the MS/AL Coast and Tampa Bay clusters.

4 Discussion

This study characterizes compound coastal flooding along the Gulf and Southeastern U.S. coasts over 2010-2024 using a nonstationary detection framework. About 37,847 flood events were identified and classified across 72 paired USGS-NOAA stations. These station-level records correspond to approximately 767 unique storm events (1-day temporal grouping window) in the study domain. Validation of 37,847 compound coastal flood events was conducted against two independent flood databases at the station level to preserve the spatial and temporal specificity of each threshold exceedance

record. Cross-referencing against the FEMA National Flood Insurance Program (NFIP) paid building claims database, which records verified economic flood losses at precise building locations, yielded a compound event match rate of 86.1% at 50 km radius (±3 days), compared to 61.1% overall and 47.6% for surge-only events. Annual NFIP match rates were highest in 2017 (78.6%) and 2021 (73.2%), coinciding with the major compound flood driven by Hurricanes Harvey/Irma/Maria and Ida respectively, providing independent temporal corroboration that the detection framework captures real compound flood forcing. Second cross-referencing against the NOAA Storm Events Database, which records flood events reported by National Weather Service offices, yielded an overall match rate of 13.1% (±3 days & 50-km radius) and 42.4% for compound events specifically. The five-type surge-discharge interaction taxonomy presented in this study, comprising surge-only, riverine-only, compound-synchronous, compound-lagged, and compound-antecedent episodes, reveals that compound coastal flooding along the Gulf and Southeastern U.S. Coasts is not a single phenomenon but a family of physically distinct processes (Fig. 3). The spatial distribution, timing structure, and intensity of these processes are governed by the interaction between storm forcing and catchment response timescales, a pattern consistent with the sub-regional hydrological controls documented along the US Gulf and Atlantic coasts (Couasnon et al., 2020; Ghanbari et al., 2021; Gori & Lin, 2022; Nasr et al., 2021; Wahl et al., 2015).

Figure 4 represents the proportional composition of compound coastal flood types across the sub-regions. The results reveal that the domain is dominated by surge-only (58.7%) followed by riverine-only (31.4%) and then compound coastal flood events (9.9%). Pascagoula-Mobile-Tombigbee recorded the highest compound fraction (17.9%) with synchronous events accounting for 90% of compound occurrences, consistent with (Ghanbari et al., 2021), who identified the western Gulf Coast as having the highest compound coastal-riverine flood probability in the contiguous US. The dominance of synchronous rather than lagged events, despite large basin areas that might otherwise promote routing delays, suggests that major Gulf-landfalling systems generate sufficiently intense and spatially coherent precipitation to synchronize fluvial and coastal peaks within the ±1 day window (Bilskie & Hagen, 2018; Gori & Lin, 2022). In contrast, Florida Panhandle exhibits the highest lagged compound fraction (19%), reflecting longer routing distances, low-gradient channels, extensive floodplain storage, and tidal backwater effects that collectively delay discharge peaks well after surge recession (Moftakhari et al., 2017; Dykstra & Dzwonkowski, 2020; Couasnon et al., 2020). This is additionally influenced by reduced exposure to direct major landfalls relative to Pascagoula-Mobile-Tombigbee. Peace-Tampa Bay exhibits the lowest compound fraction (6.9%) despite containing 65.2% of all flood events, a consequence of the shallow Gulf shelf and enclosed bay geometry amplifying surge threshold exceedances (Irish et al., 2008; Weisberg & Zheng, 2006) while small, low-relief catchments limit concurrent riverine response. This spatial anti-correlation between flood event density and compound fraction underscores the necessity of sub-regional disaggregation when interpreting compound flood dynamics across heterogeneous gauge networks. SE Atlantic Coast is typologically distinct, exhibiting the most balanced surge-riverine distribution (48%-42%) driven by a broader range of precipitation-generating systems including nor'easters and extratropical cyclones (Ghanbari et al., 2021; Nederhoff et al., 2024), and the highest antecedent compound fraction (~9.7%) attributable to the low-gradient, wetland-dominated hydrology of the St. Johns and Altamaha-St. Mary's watersheds where prolonged baseflow persistence allows discharge to precede surge by several days (Bevacqua et al., 2019). Collectively, these findings demonstrate that compound flood typology is shaped not only by storm characteristics but by the interaction between coastal forcing and watershed response timescales. The annual compound fraction ranged from 4.6% to 17.9% - a nearly four-fold range which is physically consistent with the episodic, event-driven nature of

surge-discharge co-occurrences (Figure 5) (Wahl et al., 2015; Gori et al., 2022). The five elevated years: 2012 (15.5%), 2017 (17.9%), 2020 (11.8%), 2021 (13.5%), 2024 (13.0%), correspond directly to anomalously active or impactful hurricane seasons. Notably, 2017 recorded both the highest compound fraction and the lowest total event count (1,985). The distinct peaks corresponded to active Atlantic and Gulf hurricane seasons: 2012 (15.5%; fifth most active; Hurricanes Beryl, Ernesto, and Isaac), 2017 (17.9%; extremely active and costliest season; Hurricanes Harvey, Irma, and Maria), 2020 (most active season on record; Hurricanes Sally, Zeta, and Eta), 2021 (13.5%; Hurricane Ida and Tropical Storm Elsa), and 2024 (13%; Hurricanes Helen and Milton) (Colorado State University, 2024). The lowest compound fractions coincided with below-average or near-average seasons (2010: 5.6%; 2015: 4.6%; 2022: 5.4%). Overall, the results demonstrate that compound flooding is episodic and highly variable, with certain years contributing disproportionately to compound flood occurrence. Additionally, compound flooding constitutes a distinct hazard class that is not directly inferable from total flood frequency.

Figure 6a exhibits the trimodal mean δt structure: synchronous ($\delta t \approx 0$), lagged (+2.28 days), antecedent (-2.90 days), which is physically consistent with the sub-regional typology patterns. The lagged mode's unusually low standard deviation (0.58 days) implies that in the Southeast Atlantic-Gulf Coast catchments, the delayed riverine flood peak arrives consistently about 2 days after surge, suggesting a predictable 48-hour flood advisory window following confirmed surge. The antecedent distribution's wider spread (std = 1.45 days) reflects storage-controlled rather than routing-controlled timing, consistent with SE Atlantic Coast's extended hydrological memory. The duration hierarchy surge-only (1 days) < riverine-only (2 days) < synchronous (3 days) < antecedent (5 days) < lagged (6 days) reflects progressive compounding of driver persistence timescales (Fig. 7b&c). The lagged subtype's maximum recorded duration of 14 days, the highest in the record, arises directly from its sequential flooding structure: the flood episode must span from the initial surge exceedance, through the delayed riverine peak arriving ~2 days later, and through its full recession, with no recovery period between the two flood pulses. The aggregate compound duration of 3.7 days versus 1.38 days for surge-only events (~3 times) imply that conventional univariate frameworks systematically underestimate cumulative inundation exposure associated with compound events of equivalent peak magnitude. The spatial distribution of mean δt reveals a predominantly river-first signal across the study area (Fig. 7). The near-universal river-first δt signal (station mean = +0.53 days) and the positive but marginally non-significant relationship ($r = +0.21$, $p = 0.082$) confirm routing distance as a first-order timing control (Couasnon et al., 2020), while the outlier behavior of station 2330400 (+2.14 days at only ~20 km from coast) and the three surge-first Tampa Bay stations confirm that gauge positioning within the tidal-fluvial transition zone ultimately governs compound event timing at the individual station level (Moftakhari et al., 2017). The spatial distribution of mean I_{joint} reveals two distinct hotspot zones across the study domain (Fig. 8). The Pascagoula-Mobile-Tombigbee Coast hotspot (peak $I_{joint} = 1.49$) reflects the convergence of direct Gulf-landfalling TC exposure and large drainage areas generating discharge extremes capable of substantially exceeding riverine thresholds (Ghanbari et al., 2021; Ward et al., 2018). The SE Atlantic secondary hotspot (peak $I_{joint} = 1.29$) is sustained by the disproportionate riverine contribution from low-gradient karst hydrology, consistent with SE Atlantic's elevated antecedent fraction. The Peace-Tampa Bay sub-region's low I_{joint} (approximately 0.4-0.7) despite the highest flood event count confirms that surge frequency and joint intensity are spatially anti-correlated, reinforcing that compound flood risk assessment requires both frequency and intensity metrics simultaneously, as either alone mischaracterizes the hazard at network scale.

Despite its contributions, this study has several limitations. The 15-year record is insufficient for robust trend detection against the high interannual variability characteristic of cyclone-influenced compound flood events. The 50 km USGS-NOAA pairing criterion, while consistent with prior compound flood studies, may exclude physically relevant station pairs in complex estuarine geometries where surge influence extends beyond this distance. The nonstationary 97th percentile threshold, while assumption-free and computationally consistent, does not distinguish between threshold exceedances driven by long-term sea level rise trends. Future work should extend the observational record, incorporate hydrodynamic modelling to resolve compound flood interactions at ungauged locations, and apply the five-type taxonomy to projected future climate conditions to assess how sub-regional compound flood typology may shift under sea level rise and changing tropical cyclone characteristics.

5 Conclusions

This study presents a systematic observation-based characterization of compound coastal flooding across the Gulf-Southeast coast of the United States from 2010 to 2024 using a nonstationary detection framework and a five-type surge-discharge interaction typology. The results exhibit that while surge-only and riverine-only events dominate the overall flood record, compound coastal flooding represents a distinct and physically heterogeneous hazard, accounting for 10% of detected flood events, with strong spatial and temporal variability across sub-regions. The findings reveal that compound flood occurrence is not simply proportional to total flood frequency; instead, it is governed by the interaction among storm characteristics, coastal geometry, watershed size, routing distance, and hydrologic memory.

A major contribution of this study is the identification of distinct compound coastal flood typologies based on timing lag, including synchronous, lagged, and antecedent events, each reflecting different physical mechanisms and response timescales. The Pascagoula-Mobile-Tombigbee region emerged as a key hotspot for synchronous compound flooding, while the Florida Panhandle showed a greater tendency toward lagged events and the Southeast Atlantic Coast exhibited stronger antecedent behavior. The timing and duration analyses further demonstrate that compound events persist substantially longer than surge-only floods, implying greater cumulative exposure and recovery challenges. These findings highlight the need to move beyond univariate flood assessments and incorporate both frequency and joint intensity when evaluating coastal flood risk.

Overall, these findings strengthen the observational foundation for compound flood risk assessment in one of the most flood-exposed coastal regions in the United States. By linking event typology, timing structure, spatial variability, and observed flood impacts across a large regional gauge network, this study provides a physically interpretable framework for understanding where and how compound coastal flood hazards emerge. This framework can support targeted early warning protocols, improved infrastructure design standards, and more effective adaptation planning under continued sea level rise and projected intensification of hurricane activity.

6 References

Ali, J., Wahl, T., Morim, J., Enriquez, A., Gall, M., & Emrich, C. T. (2025). Multivariate compound events drive historical floods and associated losses along the U.S. East and Gulf coasts. *Npj Natural Hazards*, *2*(1), 19. https://doi.org/10.1038/s44304-025-00076-5

Bevacqua, E., Maraun, D., Hobæk Haff, I., Widmann, M., & Vrac, M. (2017). Multivariate statistical modelling of compound events via pair-copula constructions: Analysis of floods in Ravenna (Italy). *Hydrology and Earth System Sciences*, *21*(6), 2701–2723. https://doi.org/10.5194/hess-21-2701-2017

Bevacqua, E., Maraun, D., Vousdoukas, M. I., Voukouvalas, E., Vrac, M., Mentaschi, L., & Widmann, M. (2019). Higher probability of compound flooding from precipitation and storm surge in Europe under anthropogenic climate change. *Science Advances*, *5*(9), eaaw5531. https://doi.org/10.1126/sciadv.aaw5531

Bevacqua, E., Vousdoukas, M. I., Zappa, G., Hodges, K., Shepherd, T. G., Maraun, D., Mentaschi, L., & Feyen, L. (2020). More meteorological events that drive compound coastal flooding are projected under climate change. *Communications Earth & Environment*, *1*(1), 47. https://doi.org/10.1038/s43247-020-00044-z

Bilskie, M. V., & Hagen, S. C. (2018). Defining Flood Zone Transitions in Low-Gradient Coastal Regions. *Geophysical Research Letters*, *45*(6), 2761–2770. https://doi.org/10.1002/2018GL077524

Couasnon, A., Eilander, D., Muis, S., Veldkamp, T. I. E., Haigh, I. D., Wahl, T., Winsemius, H. C., & Ward, P. J. (2020). Measuring compound flood potential from river discharge and storm surge extremes at the global scale. *Natural Hazards and Earth System Sciences*, *20*(2), 489–504. https://doi.org/10.5194/nhess-20-489-2020

Dykstra, S. L., & Dzwonkowski, B. (2020). The Propagation of Fluvial Flood Waves Through a Backwater-Estuarine Environment. *Water Resources Research*, *56*(2), e2019WR025743. https://doi.org/10.1029/2019WR025743

Eilander, D., Couasnon, A., Ikeuchi, H., Muis, S., Yamazaki, D., Winsemius, H. C., & Ward, P. J. (2020). The effect of surge on riverine flood hazard and impact in deltas globally. *Environmental Research Letters*, *15*(10), 104007. https://doi.org/10.1088/1748-9326/ab8ca6

Ezer, T., & Atkinson, L. P. (2014). Accelerated flooding along the U.S. East Coast: On the impact of sea-level rise, tides, storms, the Gulf Stream, and the North Atlantic Oscillations. *Earth's Future*, *2*(8), 362–382. https://doi.org/10.1002/2014EF000252

FEMA (2026). OpenFEMA Dataset: FIMA NFIP Redacted Claims - v2. Federal Emergency Management Agency. Available at: https://www.fema.gov/openfema-data-page/fima-nfip-redacted-claims-v2 [Accessed: April 2026].

Ghanbari, M., Arabi, M., Kao, S.-C., Obeysekera, J., & Sweet, W. (2021). Climate Change and Changes in Compound Coastal-Riverine Flooding Hazard Along the U.S. Coasts. *Earth's Future*, *9*(5), e2021EF002055. https://doi.org/10.1029/2021EF002055

Gori, A., & Lin, N. (2022). Projecting Compound Flood Hazard Under Climate Change With Physical Models and Joint Probability Methods. *Earth's Future*, *10*(12), e2022EF003097. https://doi.org/10.1029/2022EF003097

Gori, A., Lin, N., & Smith, J. (2020). Assessing Compound Flooding From Landfalling Tropical Cyclones on the North Carolina Coast. *Water Resources Research*, *56*(4), e2019WR026788. https://doi.org/10.1029/2019WR026788

Green, J., Haigh, I. D., Quinn, N., Neal, J., Wahl, T., Wood, M., Eilander, D., de Ruiter, M., Ward, P., & Camus, P. (2025). Review article: A comprehensive review of compound flooding literature with a focus

on coastal and estuarine regions. *Natural Hazards and Earth System Sciences*, *25*(2), 747–816. https://doi.org/10.5194/nhess-25-747-2025

Irish, J. L., Resio, D. T., & Ratcliff, J. J. (2008). *The Influence of Storm Size on Hurricane Surge*. https://doi.org/10.1175/2008JPO3727.1

Juárez, B., Stockton, S. A., Serafin, K. A., & Valle-Levinson, A. (2022). Compound Flooding in a Subtropical Estuary Caused by Hurricane Irma 2017. *Geophysical Research Letters*, *49*(18), e2022GL099360. https://doi.org/10.1029/2022GL099360

Leonard, M., Westra, S., Phatak, A., Lambert, M., van den Hurk, B., McInnes, K., Risbey, J., Schuster, S., Jakob, D., & Stafford-Smith, M. (2014). A compound event framework for understanding extreme impacts. *WIREs Climate Change*, *5*(1), 113–128. https://doi.org/10.1002/wcc.252

Li, H., Jane, R. A., Eilander, D., Enríquez, A. R., Haer, T., & Ward, P. J. (2026). Assessing the spatial correlation of potential compound flooding in the United States. *Natural Hazards and Earth System Sciences*, *26*(1), 391–409. https://doi.org/10.5194/nhess-26-391-2026

Little, C. M., Horton, R. M., Kopp, R. E., Oppenheimer, M., Vecchi, G. A., & Villarini, G. (2015). Joint projections of US East Coast sea level and storm surge. *Nature Climate Change*, *5*(12), 1114–1120. https://doi.org/10.1038/nclimate2801

Moftakhari, H. R., Salvadori, G., AghaKouchak, A., Sanders, B. F., & Matthew, R. A. (2017). Compounding effects of sea level rise and fluvial flooding. *Proceedings of the National Academy of Sciences*, *114*(37), 9785–9790. https://doi.org/10.1073/pnas.1620325114

Moftakhari, H., Schubert, J. E., AghaKouchak, A., Matthew, R. A., & Sanders, B. F. (2019). Linking statistical and hydrodynamic modeling for compound flood hazard assessment in tidal channels and estuaries. *Advances in Water Resources*, *128*, 28–38. https://doi.org/10.1016/j.advwatres.2019.04.009

Muñoz, D. F., Moftakhari, H., & Moradkhani, H. (2020). Compound Effects of Flood Drivers and Wetland Elevation Correction on Coastal Flood Hazard Assessment. *Water Resources Research*, *56*(7), e2020WR027544. https://doi.org/10.1029/2020WR027544

Muñoz, D. F., Muñoz, P., Moftakhari, H., & Moradkhani, H. (2021). From local to regional compound flood mapping with deep learning and data fusion techniques. *Science of The Total Environment*, *782*, 146927. https://doi.org/10.1016/j.scitotenv.2021.146927

Nasr, A. A., Wahl, T., Rashid, M. M., Camus, P., & Haigh, I. D. (2021). Assessing the dependence structure between oceanographic, fluvial, and pluvial flooding drivers along the United States coastline. *Hydrology and Earth System Sciences*, *25*(12), 6203–6222. https://doi.org/10.5194/hess-25-6203-2021

Nederhoff, K., Leijnse, T. W. B., Parker, K., Thomas, J., O'Neill, A., van Ormondt, M., McCall, R., Erikson, L., Barnard, P. L., Foxgrover, A., Klessens, W., Nadal-Caraballo, N. C., & Massey, T. C. (2024). Tropical or extratropical cyclones: What drives the compound flood hazard, impact, and risk for the United States Southeast Atlantic coast? *Natural Hazards*, *120*(9), 8779–8825. https://doi.org/10.1007/s11069-024-06552-x

NOAA National Centers for Environmental Information (2024). Storm Events Database. National Oceanic and Atmospheric Administration. Available at: https://www.ncdc.noaa.gov/stormevents/ [Accessed: March 2026].

NOAA, Center for Operational Oceanographic Products and Services. (2026). *NOAA Tides and Currents Data API.* Retrieved from NOAA Tides and Currents.

Raymond, C., Horton, R. M., Zscheischler, J., Martius, O., AghaKouchak, A., Balch, J., Bowen, S. G., Camargo, S. J., Hess, J., Kornhuber, K., Oppenheimer, M., Ruane, A. C., Wahl, T., & White, K. (2020). Understanding and managing connected extreme events. *Nature Climate Change*, *10*(7), 611–621. https://doi.org/10.1038/s41558-020-0790-4

Sadegh, M., Moftakhari, H., Gupta, H. V., Ragno, E., Mazdiyasni, O., Sanders, B., Matthew, R., & AghaKouchak, A. (2018). Multihazard Scenarios for Analysis of Compound Extreme Events. *Geophysical Research Letters*, *45*(11), 5470–5480. https://doi.org/10.1029/2018GL077317

Salas, J. D., & Obeysekera, J. (2014). Revisiting the Concepts of Return Period and Risk for Nonstationary Hydrologic Extreme Events. *Journal of Hydrologic Engineering*, *19*(3), 554–568. https://doi.org/10.1061/(ASCE)HE.1943-5584.0000820

Seneviratne, S. I., Zhang, X., Adnan, M., Badi, W., Dereczynski, C., Di Luca, A., Ghosh, S., Iskandar, I., Kossin, J., Lewis, S., Otto, F., Pinto, I., Satoh, M., Vicente-Serrano, S. M., Wehner, M., & Zhou, B. (2021). Weather and climate extreme events in a changing climate. In V. Masson-Delmotte, P. Zhai, A. Pirani, S. L. Connors, C. Péan, S. Berger, N. Caud, Y. Chen, L. Goldfarb, M. I. Gomis, M. Huang, K. Leitzell, E. Lonnoy, J. B. R. Matthews, T. K. Maycock, T. Waterfield, Ö. Yelekçi, R. Yu, & B. Zhou (Eds.), *Climate Change 2021: The Physical Science Basis. Contribution of Working Group I to the Sixth Assessment Report of the Intergovernmental Panel on Climate Change* (pp. 1513–1766). Cambridge University Press. https://doi.org/10.1017/9781009157896.001

Sohrabi, M., Moftakhari, H., & Moradkhani, H. (2025). Analyzing Compound Flooding Drivers Across the US Gulf Coast States. *Geophysical Research Letters*, *52*(9), e2025GL114769. https://doi.org/10.1029/2025GL114769

Sweet, W., Hamlington, B., Kopp, R. E., Weaver, C., Barnard, P. L., Bekaert, D., Brooks, W., Craghan, M., Dusek, G., Frederikse, T., Garner, G., Genz, A. S., Krasting, J. P., Larour, E., Marcy, D., Marra, J. J., Obeysekera, J., Osler, M., Pendleton, M., … Zuzak, C. (2022). Global and regional sea level rise scenarios for the United States. In *Technical Report* (NOS.01). National Oceanic and Atmospheric Administration. https://pubs.usgs.gov/publication/70229139

U.S. Geological Survey. (2026). *USGS Water Data for the Nation: U.S. Geological Survey National Water Information System database*. Retrieved from https://doi.org/10.5066/F7P55KJN

Visser-Quinn, A., Beevers, L., Collet, L., Formetta, G., Smith, K., Wanders, N., Thober, S., Pan, M., & Kumar, R. (2019). Spatio-temporal analysis of compound hydro-hazard extremes across the UK. *Advances in Water Resources*, *130*, 77–90. https://doi.org/10.1016/j.advwatres.2019.05.019

Vogel, R. M., Yaindl, C., & Walter, M. (2011). Nonstationarity: Flood Magnification and Recurrence Reduction Factors in the United States. *JAWRA Journal of the American Water Resources Association*, *47*(3), 464–474. https://doi.org/10.1111/j.1752-1688.2011.00541.x

Wahl, T., Jain, S., Bender, J., Meyers, S. D., & Luther, M. E. (2015). Increasing risk of compound flooding from storm surge and rainfall for major US cities. *Nature Climate Change*, *5*(12), 1093–1097. https://doi.org/10.1038/nclimate2736

Ward, P. J., Couasnon, A., Eilander, D., Haigh, I. D., Hendry, A., Muis, S., Veldkamp, T. I. E., Winsemius, H. C., & Wahl, T. (2018). Dependence between high sea-level and high river discharge increases flood hazard in global deltas and estuaries. *Environmental Research Letters*, *13*(8), 084012. https://doi.org/10.1088/1748-9326/aad400

Weisberg, R. H., & Zheng, L. (2006). Hurricane storm surge simulations for Tampa Bay. *Estuaries and Coasts*, *29*(6), 899–913. https://doi.org/10.1007/BF02798649

Xu, K., Wang, C., & Bin, L. (2023). Compound flood models in coastal areas: A review of methods and uncertainty analysis. *Natural Hazards*, *116*(1), 469–496. https://doi.org/10.1007/s11069-022-05683-3

Yangchen, L., Li, J., Xihui, G., Liu, C., & Chen, Y. (2021). Global compound floods from precipitation and storm surge: Hazards and the roles of cyclones. *Journal of Climate*, 1–55. https://doi.org/10.1175/JCLI-D-21-0050.1

Zscheischler, J., Martius, O., Westra, S., Bevacqua, E., Raymond, C., Horton, R. M., van den Hurk, B., AghaKouchak, A., Jézéquel, A., Mahecha, M. D., Maraun, D., Ramos, A. M., Ridder, N. N., Thiery, W., & Vignotto, E. (2020). A typology of compound weather and climate events. *Nature Reviews Earth & Environment*, *1*(7), 333–347. https://doi.org/10.1038/s43017-020-0060-z

Zscheischler, J., Westra, S., van den Hurk, B. J. J. M., Seneviratne, S. I., Ward, P. J., Pitman, A., AghaKouchak, A., Bresch, D. N., Leonard, M., Wahl, T., & Zhang, X. (2018). Future climate risk from compound events. *Nature Climate Change*, *8*(6), 469–477. https://doi.org/10.1038/s41558-018-0156-3